Neuronal wiring receptors Dprs and DIPs are GPI anchored and this modification contributes to their cell surface organization

Meike Lobb-Rabe*[,1,2,3], Wioletta I. Nawrocka*[,3,4,5], Robert A. Carrillo[1,2,3,+], and Engin Özkan[3,4,5,+]

* Authors contributed equally; order was determined by coin flip

[1] Department of Molecular Genetics and Cell Biology, University of Chicago, Chicago, Illinois 60637

[2] Program in Cell and Molecular Biology, University of Chicago, Chicago, Illinois 60637

[3] Neuroscience Institute, University of Chicago, Chicago, Illinois 60637

[4] Department in Biochemistry and Molecular Biology, University of Chicago, Chicago, Illinois 60637

[5] Institute for Biophysical Dynamics, University of Chicago, Chicago, Illinois 60637

[+] Correspondence: robertcarrillo@uchicago.edu and eozkan@uchicago.edu

ORCID IDs

Meike Lobb-Rabe ORCID ID: 0000-0001-6486-7752

Wioletta I. Nawrocka ORCID ID: 0000-0001-5019-7196

Robert A. Carrillo ORCID ID: 0000-0002-2067-9861

Engin Özkan ORCID ID: 0000-0002-0263-6729

ABSTRACT

The *Drosophila* Dpr and DIP proteins belong to the immunoglobulin superfamily of cell surface proteins (CSPs). Their hetero- and homophilic interactions have been implicated in a variety of neuronal functions, including synaptic connectivity, cell survival, and axon fasciculation. However, the signaling pathways underlying these diverse functions are unknown. To gain insight into Dpr–DIP signaling, we sought to examine how these CSPs are associated with the membrane. Specifically, we asked whether Dprs and DIPs are integral membrane proteins or membrane anchored through the addition of glycosylphosphatidylinositol (GPI) linkage. We demonstrate that Dprs and DIPs are GPI anchored to the membrane of insect cells and validate these findings for some family members in vivo using *Drosophila* larvae, where GPI anchor cleavage results in loss of surface labeling. Additionally, we show that GPI cleavage abrogates aggregation of insect cells expressing cognate Dpr–DIP partners. To test if the GPI anchor affects Dpr–DIP localization, we replaced it with a transmembrane domain and observed perturbation of sub-cellular localization on motor neurons and muscles. These data suggest that membrane anchoring of Dprs and DIPs through GPI linkage is required for localization and that Dpr–DIP intracellular signaling likely requires transmembrane co-receptors.

Keywords: Glycosylphosphatidylinositol anchor; Cell surface receptor; Dpr; DIP; Surface localization; Motor neuron; Muscle; *Drosophila melanogaster*

INTRODUCTION

Cell Surface Proteins (CSPs) allow a cell to interact with neighboring cells and the extracellular matrix and interpret chemical cues from its environment. CSPs can be attached to cells through hydrophobic transmembrane domains that traverse the lipid bilayer or via post-translational modifications that anchor the protein in the plasma membrane. One such modification is the addition of a glycosylphosphatidylinositol (GPI) anchor, which is covalently linked to the C-terminus of the protein and embeds its hydrophobic acyl chains into the outer leaflet of the cell membrane.[1–3] GPI anchors are attached at the ω site, typically a small amino acid, flanked upstream by an unstructured region and downstream by a stretch of hydrophobic residues.[4] The GPI anchor is added in the ER lumen during protein synthesis, and the mature protein is trafficked to the cell membrane through the secretory pathway.[5] GPI-anchored proteins cannot signal into the cells directly, as the anchors do not physically reach into the cell interior. Thus, the interaction of GPI linked proteins with intracellular signaling pathways likely requires engagement of transmembrane co-receptors able to transduce the signal inside the cell.

The human genome is predicted to encode at least 129 GPI-anchored proteins.[6] These include molecules implicated in a variety of functions in the nervous system including axon guidance and synaptic adhesion (reviewed in Um and Ko, 2017)[7]. Abrogation of GPI anchoring and defects in biosynthesis of GPI anchors have been implicated in various diseases including central nervous system disorders.[8,9]

Computational tools to predict GPI-anchored proteins have been unreliable due, in part, to small training sets and similarity of features associated with GPI anchors and transmembrane domains. Compounding issues with predictions, the membrane-

anchoring status of a particular protein cannot simply be deduced from its homology with other proteins; protein families may include members that can be transmembrane, GPI anchored and secreted. For example, the Semaphorin family of key axon guidance cues includes members that are secreted (classes 2 and 3), transmembrane (classes 1, 4, 5, 6) and GPI anchored (class 7).[10] Sema7A is GPI anchored and involved in axonal outgrowth,[11] synaptic pruning,[12] and integrin-dependent stimulation of immune cells.[13] Ephrins, the membrane-tethered ligands for the receptor tyrosine kinases, Ephs, are divided into GPI anchored ephrin-A and single-pass transmembrane ephrin-B classes and act by binding their cognate EphA and EphB receptors, respectively.[14,15] Interestingly, GPI-anchored Ephrin-A5 has been shown to transmit an intracellular signal despite the lack of intracellular region; it partitions into caveolae-like microdomains and engages Fyn protein tyrosine kinase signaling upon interaction with an externally applied soluble form of EphA5 receptor.[16]

The IgLONs, a five-member family of conserved mammalian CSPs, are GPI anchored and function in neurite outgrowth and synaptogenesis.[17–20] IgLON-mediated signaling remains poorly understood although one member, Negr1, is cleaved by an ADAM-family protease and binds to an FGF receptor to stimulate dendritic arbor growth.[21] The *Drosophila melanogaster* orthologs of the IgLONs, the Dpr–DIP family of CSPs,[22] have been implicated in a variety of functions, including synapse specificity and partner preference,[23–28] axonal pathfinding and fasciculation,[29–31] cell fate determination,[25] cell survival,[24,28,32], and behavior.[33] Structurally, the ectodomains of Dprs and DIPs consist of two and three immunoglobulin (Ig) domains, respectively,[24,34] similar to IgLONs which have three Ig domains and interact in a structurally similar

manner to Dprs and DIPs.[22,35] However, how these proteins are linked to the cell membrane has not been determined. Here, we tested whether members of the *Drosophila* Dpr/DIP family are GPI anchored. We observed that all Dprs and DIPs have a GPI anchor; this was not expected as only a few family members are predicted to have GPI anchors. Treatment with GPI-specific phospholipase-C (PLC) causes shedding of Dprs and DIPs from the surface of insect cells and live fly tissue; this cleavage is GPI anchor-dependent, as it is lost when the GPI anchor site is replaced with a transmembrane domain of a CD4 glycoprotein. Additionally, cleavage of GPI anchors also abolishes Dpr–DIP-mediated cell aggregation. Finally, replacing the GPI anchor with a transmembrane domain perturbs presynaptic and postsynaptic localization of these CSPs. Together these findings suggest that GPI anchors of Dpr/DIP contribute to their localization and function.

RESULTS

Some Dprs and DIPs are predicted to be GPI anchored

The Dprs and DIPs bind selectively with one another via their ectodomains, forming an elaborate network of homo- and heterophilic interactions (Figure 1A). Their multifunctional roles in neural circuit development partially relies on their abilities to act as cell adhesion molecules. However, whether and how Dprs and DIPs signal intracellularly has not been examined. Determining if they are transmembrane (TM) or GPI anchored proteins would shed light on their potential signaling mechanisms.

To gain insight into how Dprs and DIPs associate with the cell membrane we used two transmembrane region prediction tools, Phobius[36] and DeepTMHMM[37]. We

first removed N-terminal signal peptides recognized by SignalP-6.0[38] to avoid their classification as TM domains, which is an inherent challenge for TM region prediction tools due to the hydrophobic nature of both types of sequences. Phobius predicted 15 of the Dprs and DIPs and Klingon to have C-terminal TM regions while DeepTMHMM indicated only Dpr9 as a TM protein (Figure S1).

Next, we hypothesized that those Dprs and DIPs that were not classified as transmembrane may be anchored to the membrane via GPI modification (Figure 1B). We used two GPI signal prediction tools, PredGPI[39] and NetGPI[40]. PredGPI predicts the likelihood that a protein is GPI anchored and the position of the ω site—the residue to which the lipid anchor is attached. PredGPI is based on Hidden Markov Model, trained on experimentally validated GPI anchored proteins, and produces minimal false positives while correctly identifying 89% of known GPI-containing proteins. NetGPI is a more recently developed prediction software that uses neural networks to predict GPI anchoring, the ω site, and the likelihood of the selected position being correct. NetGPI was reported to slightly outperform PredGPI.[40]

We examined all 32 members of the Dpr/DIP family and Klingon, an immunoglobulin superfamily (IgSF) protein previously demonstrated to be GPI anchored,[41] with PredGPI and NetGPI and the majority of these CSPs were predicted to lack GPI anchors (Figure 1C and Table S2). PredGPI indicated 8 Dprs and DIPs (25%) as likely GPI linked (specificity above 99%) and Klingon as not GPI anchored as it fell under the threshold for positivity with its specificity value of 98.5%. NetGPI predicted 11 Dprs and DIPs (34%) to be GPI anchored and correctly classified Klingon. Among the proteins predicted to have a GPI modification by NetGPI, 67% were also predicted by

PredGPI. Surprisingly, Dpr3, Dpr5, and DIP-η were classified by NetGPI as likely GPI anchored, but obtained very low specificity index values of 37.30%, 16.00%, and 1.00%, respectively with PredGPI.

Overall, 12 Dprs and DIPs were predicted to be GPI anchored by either PredGPI or NetGPI (Figure S2). 15 Dprs and DIPs were predicted to have TM helices, and five of these CSPs were also predicted to have a GPI anchor (Dpr5, Dpr11, DIP-γ, DIP-ζ, and DIP-η). Ten Dprs and DIPs were not predicted to be GPI linked nor to contain a TM helix (Dpr4, Dpr6, Dpr10, Dpr13, Dpr15, Dpr16, Dpr17, DIP-θ, DIP-ι). Thus, using prediction tools alone did not unequivocally classify how these CSPs are anchored to the cell.

Dprs and DIPs are anchored to the membrane via glycophosphatidyl linkages

To complement the prediction tools and examine the membrane anchoring mechanism(s) of all Dprs and DIPs, we setup an S2 cell culture pipeline with V5-tagged, full-length proteins (see Table 1 and the methods section for details). Duplicate S2 cultures were established for each CSP, and one culture was treated with the GPI cleaving enzyme Phospholipase C (PLC). Supernatant and cell fractions were collected and used for western blot analyses to determine if the CSP was cleaved by PLC. The GPI-anchored protein Klingon was used as the positive control and the secreted cDIP and transmembrane proteins Roughest (Rst) and Kirre served as negative controls.[24,41–43] If the CSPs are GPI anchored, we expect an increase of protein in the supernatant and a concomitant decrease in the cell fraction after PLC treatment (Figure 2A). Remarkably, all Dprs and DIPs displayed these trends, suggesting that, like their

vertebrate orthologs, the IgLONs, Dprs and DIPs are GPI anchored (Figure 2B).

We next used flow cytometry as an orthogonal method to demonstrate the GPI anchoring of Dprs and DIPs. We expressed the same, N-terminally V5-tagged constructs of three Dprs and three DIPs in Sf9 cells using baculoviral infection. The cultures expressing individual Dprs and DIPs, as well as the negative control, Rst, were split into two samples: one was treated with PLC, and the other served as an untreated control. Both samples were stained with fluorescent antibodies against V5 tag and the relative levels of proteins on the surface of PLC-treated and untreated cells were assessed using a flow cytometer. All DIPs tested, DIP-α, DIP-β, and DIP-γ, showed a significant decrease in protein levels on the surface of Sf9 cells after PLC treatment (Figure 3A-C). Similarly, all Dprs tested, Dpr10, Dpr11, and Dpr21, were mostly cleaved off the cell surface by PLC (Figure 3D-F). In contrast, the level of Rst on the cell surface remained unaffected by PLC cleavage (Figure 3G-H), as expected for a transmembrane protein. The differential extent of cleavage between all tested Dprs and DIPs could be explained by the potentially different accessibility of the GPI cleavage site for each of the proteins. The results obtained using flow cytometry corroborate the observations made using western blot analyses. Together, these findings demonstrate that Dprs and DIPs are GPI anchored.

GPI anchor cleavage eliminates Dpr–DIP-mediated cell aggregation

Dprs and DIPs are thought to mediate cell adhesive interactions to accomplish many of their roles in the nervous system.[32] A powerful in vitro approach to study cell adhesion interactions is the cell aggregation assay.[44–46] Here, we combined cell

aggregation and PLC assays to test whether cleavage of GPI anchors abrogates cell adhesion mediated by Dprs and DIPs. We used Sf9 cells infected with baculoviruses encoding mScarlet or EGFP followed by V5-tagged, full-length Dpr or DIP, respectively, separated by a P2A peptide. We confirmed the expression of Dprs and DIPs using western blots with an anti-V5 antibody (Figure S3). Cultures expressing individual Dprs with mScarlet were mixed with cultures expressing cognate DIP partners and EGFP. We predicted that, if Dprs and DIPs are GPI-anchored cell adhesion molecules, Dpr–DIP interactions would lead to aggregation between the respective cells, and application of PLC would break up the aggregates. Among the four pairs of cognate Dprs and DIPs tested, DIP-α and Dpr6, DIP-β and Dpr10, and DIP-γ and Dpr11 induced robust aggregation of Sf9 cells (Figure 4A-E). DIP-β and Dpr21-expressing cells aggregated significantly less, which was surprising considering their relatively high affinity compared to other Dpr–DIP pairs,[47] and that the expression levels of DIP-β and Dpr21 were comparable to other proteins tested here. One reason for the reduced aggregation may be weak homophilic Dpr21 interactions (K_D ~ 50 uM) on the same cell that may prevent efficient heterophilic interactions with DIP-β between cells, as homophilic and heterophilic complexes use the same interfaces and cannot co-exist.[47,48] Nonetheless, the addition of PLC significantly reduced cell aggregation for all four pairs of Dprs and DIPs. These results demonstrate that Dpr–DIP interactions instruct cell adhesion and suggest that Dprs and DIPs are anchored to the cell surface membrane via GPI modifications.

Dpr and DIP proteins are GPI anchored in vivo

Having demonstrated that Dprs and DIPs are GPI anchored in vitro, we wanted to determine if the same modification occurs in fly tissue. We expressed tagged forms of Dprs and DIPs in the neuromuscular circuit using the GAL4-UAS system. The larval *Drosophila* neuromuscular junction (NMJ) is an excellent system to examine cell surface proteins, as the circuit is well characterized and easily imaged. Moreover, Dprs and DIPs are endogenously expressed at the larval NMJ,[49] and several Dprs and DIPs are implicated in NMJ development. DIP-α and Dpr10 are known to function in motor axon pathfinding and innervation,[23,31] and DIP-γ and Dpr11 regulate synaptic growth through the BMP pathway.[24]

To achieve high protein levels in a cell type that would allow for easy visualization of Dprs and DIPs on the cell surface, we expressed proteins in muscles using *Mef2-GAL4* and omitted detergents in the initial steps of our staining protocol. Muscles are highly stereotyped, multinucleated cells that are easily imaged. In third instar larvae, V5-Dpr19 localized to the subsynaptic reticulum (SSR), a network of postsynaptic membrane folds surrounding the innervating presynaptic boutons (Figure 5A-B). After incubation with PLC, nearly all surface V5 signal was lost, indicating that Dpr19 is GPI anchored in vivo (Figure 5M). Similarly, V5-Dpr10 was localized to the SSR and PLC treatment significantly decreased the V5 signal (Figure 5C-D,N). However, unlike Dpr19, significant Dpr10 remained on the muscle surface in puncta surrounding boutons (Figure 5D,D'), suggesting that a population of Dpr10 was inaccessible to PLC or prevented from diffusing away by interacting with other CSPs at these sites. To confirm that loss of the cell surface signal was due to cleavage of the GPI anchor, we generated chimeric transmembrane tethered Dpr10 proteins by

replacing the second Ig domain and C-terminus of Dpr10 with the fourth Ig and transmembrane domains of CD4 (a transmembrane protein not endogenously found in flies). As expected, the cell surface abundance of this chimeric Dpr10-CD4 was unaffected after PLC treatment, suggesting that Dpr10 is anchored at the NMJ via GPI modification (Figure 5E-F',O). Conversely, when we replaced Ig1 of Dpr10 with the first Ig domain of CD4 but retained the second Ig and C-terminus, this chimeric CD4-Dpr10 was efficiently released from the muscle surface by PLC (Figure 5G-H',P), indicating that some PLC-released Dpr10 was likely retained on the cell surface through its adhesion domain, Ig1, via interactions with endogenous Dprs and DIPs. These results demonstrate that Dpr10 and Dpr19 are GPI anchored in their endogenous tissue.

Next, we examined two DIPs, DIP-α and DIP-ζ. Although neither is endogenously expressed in muscles,[49] an ectopically expressed DIP-α variant localized to the SSR (Figure 5I). Like Dpr10 and Dpr19, DIP-α was released from the muscle surface after PLC treatment (Figure 5I-J',Q). However, cleavage was less efficient, and DIP-α puncta formed on the muscle surface and around boutons after treatment. Similar to Dpr10, replacing Ig2-Ig3 and the C-terminus of DIP-α with CD4 blocked the PLC-mediated release from the muscle surface (Figure 5K-L',R). Strikingly, DIP-ζ did not localize to the SSR, and PLC treatment resulted in increased DIP-ζ puncta across the muscle surface (Figure S4A-C). Overall, these data show that PLC treatment affects Dpr10, DIP-α and -ζ attachment and localization in vivo and support our model that Dprs and DIPs are GPI anchored CSPs.

GPI anchor alters localization in neurons and muscle cells

GPI modifications have been shown to contribute to the subcellular localization of CSPs.[50,51] Thus, we examined localization of ectopically expressed wild type and chimeric Dpr10 and DIP-α in their endogenous tissues. DIP-α is expressed in a subset of motor neurons called the Is type and localizes to the axon terminals.[23,24,49] Using a Is motor neuron-specific driver, *A8-GAL4*,[27,52] we confirmed that Myc-DIP-α localizes to puncta in the motor axon terminal (Figure 6A-B'). However, when the GPI anchor was replaced with a TM domain, DIP-α was redistributed and fewer puncta formed, suggesting that clustered presynaptic localization is partially due to the GPI anchor (Figure 6C-D'). These changes were confirmed by quantifying DIP-α puncta in the terminal three boutons in each condition: In order to determine the nature of this localization difference, samples were thresholded and collapsed to a binary representation (Figure 6B,D), and then the number of particles in and around the three terminal boutons of each arbor were quantified. Myc-DIP-α formed more and smaller puncta compared to DIP-α-CD4 (Figure 6I-J), suggesting that the GPI anchor contributes to the subcellular localization of DIP-α in vivo.

As described above, expressing Dpr10 in muscles results in Dpr10 localization at the SSR, the membrane folds that form around in presynaptic boutons. However, additional puncta are observable away from boutons on the muscle surface (Figure6 E-H') and these puncta were significantly reduced when compared to the localization of the chimeric DIP-α containing a transmembrane helix (Figure6 K-L). Taken together, GPI anchors of DIP-α and Dpr10 contribute to both their pre- and postsynaptic localization, respectively.

DISCUSSION

Dprs and DIPs have been implicated in many aspects of neural circuit development. However, we lack a systematic analysis of how these CSPs are anchored to the cell membrane to provide insights into their signaling mechanisms. Here, we utilize several in vitro and in vivo approaches to demonstrate that all Dprs and DIPs are attached to the cell membrane through GPI anchors. In tissue, we show that GPI anchors contribute to subcellular clustering on the presynaptic neuronal membrane. Our findings, that all Dpr and DIPs are GPI anchored, suggest that Dpr/DIP-mediated functions must be achieved either by merely tethering two cells together and/or by signaling through a co-receptor.

Predicting GPI anchors

Predicting GPI anchors is intrinsically challenging for multiple reasons. First, the features that predispose the protein to GPI anchor attachment are not very well defined. Second, the ω site is flanked downstream by a stretch of hydrophobic amino acids that can resemble a single-pass transmembrane domain. Third, it is estimated that the animal genomes may each encode over 100 GPI anchored proteins, but only a fraction of those have been experimentally validated, resulting in limited training datasets for prediction tools. Consequently, both currently annotated GPI-anchored proteins and the predictions of such proteins likely represent an underestimate of the actual number. Indeed, a high number of false negatives was observed in this study, as only one-third of Dprs and DIPs were predicted to be GPI anchored by the latest available algorithms in PredGPI and NetGPI. Conversely, the TM prediction tool Phobius predicted 15 out of

32 Dprs and DIPs and Klingon as TM proteins, suggesting this software may not be robust at discriminating between the two membrane targeting motifs. This is not surprising, however, considering the similar chemical nature of TM helices and GPI signals. The newest version of TMHMM, DeepTMHMM, a deep learning-based algorithm, performed significantly better than Phobius, classifying only Dpr9 as a TM protein. Unexpectedly, one-third of Dprs and DIPs were neither predicted to be GPI anchored nor to have a TM helix. Together our findings demonstrate that currently available GPI signal prediction tools can provide useful preliminary insights, especially in combination with TM prediction software. However, experimental validation should be the primary way of assessing GPI anchor presence, when possible, until better prediction tools are developed.

Dpr and DIP clustering is aided by their GPI anchors

CSP localization is often critical for their function. Here, we demonstrate that DIP-α, Dpr10, and Dpr19 localized to the postsynaptic membrane when expressed in muscles. Moreover, punctate Dpr10 localization on the muscle surface was diminished when we replaced the GPI anchor with a TM helix suggesting that this modification contributes to its localization. Similar results were observed for punctate DIP-α in presynaptic Is arbors. GPI-anchored proteins have been reported to localize to lipid rafts—domains in the lipid bilayer that have increased levels of sterols and are therefore slightly thicker and less mobile than the surrounding membrane.[53] Although still somewhat controversial, these domains are thought to scaffold proteins by increasing the local concentration of proteins that preferentially localize to lipid rafts such as GPI-

anchored proteins, possibly including Dprs and DIPs within these rafts.

The PLC cleavage of Dpr10 and DIP-α from muscles was incomplete, leaving residual punctate signal around the boutons and on the muscle surface unlike Dpr19 that was almost completely lost. These differences in PLC cleavage efficiencies may be due to different local interactions of Dprs and DIPs with various proteins or lipids in the membrane. Alternatively, we provide evidence suggesting that cleavage is complete and the observed signal is due to the cleaved CSPs binding nearby proteins and preventing release from the tissue.

Dpr–DIP-mediated cell adhesion depends on their GPI anchors

Trans- and *cis*-interactions between Dprs and DIPs drive their roles in the nervous system. Dprs and DIPs may act similar to other cell adhesion molecules (e.g., integrins or cadherins) by clustering to generate avidity and strengthen cell-cell contacts during axonal fasciculation or synapse formation. We examined four Dpr–DIP pairs and all showed robust aggregation that was susceptible to PLC treatment, suggesting that the GPI anchors in Dprs and DIPs are accessible by PLC at the cell-cell contact sites. This phenomenon could have profound consequences in vivo for modulating cell adhesion, provided that specific lipases and proteases are present under physiological conditions at sufficient concentrations and exhibit high enough substrate turnover to cause structural changes to cell-cell contacts.

Shedding of cell surface molecules by hydrolytic enzymes like proteases and lipases has been implicated in various signaling mechanisms. Examples include activation of fibroblast growth factor 2 (FGF-2) via the release of soluble syndecan-1,[54]

potentiation of β-catenin signaling upon cleavage of neuronal cadherin (N-cadherin),[55] modulation of Nodal signaling via GPI cleavage of CRIPTO,[56] and bi-directional regulation of the Notch pathway through proteolysis of Notch or its ligands.[57–60] GPI-anchored proteins are unable to directly signal intracellularly so acting as soluble factors for other receptors, either in *cis* or *trans*, could be a conceivable mode of action. A subset of Dprs[61] and DIPs were identified in a secretome screen as soluble factors in the hemolymph of larvae (Personal Communication, Norbert Perrimon and Justin Bosch), but the roles of these soluble variants are unknown. In addition to potential functions of soluble forms of these CSPs in the extracellular space, it would be interesting to explore if their shedding in vivo could affect Dpr–DIP-mediated cell adhesion, and have consequences for the structure and function of synapses or other specialized sites of cell-cell contact, as shown for some CAMs.[55,62–66]

GPI anchors in neural circuit assembly

GPI-anchored proteins are critical for many physiological processes, including neural circuit formation. These proteins can be cleaved by lipases or proteases as part of their signaling mechanism. For example, the GPI-anchored protein RECK regulates motor neuron differentiation in mammals by inhibiting Notch signaling; only when RECK is cleaved and released from the membrane can the ADAM10 metalloprotease access and cleave the Notch ligand thereby promoting differentiation.[67] In addition, IgLONs, the vertebrate orthologs of Dprs and DIPs, are shed from neurons via ADAM10 to promote neuronal growth of nearby neurons.[19,21] The presence of GPI anchors in Dprs and DIPs suggests that their biology and signaling may be conserved with IgLONs. Finally, if the

GPI-anchored protein is not cleaved, it can still signal through a co-receptor that traverses the cell membrane. To our knowledge, no Dpr or DIP co-receptors have been published and this provides an intriguing future avenue of research.

Acknowledgments

We would like to thank Szymon Kordon, Ruiling Zhang, Gabriel Carmona Rosas, Indya Weathers, Stephanie Dunning, Veera Anand, and Yupu Wang as well as members of the Carrillo and Özkan Labs for support and feedback. This work is supported by NINDS R01 NS123439 and a UChicago Faculty Diversity Grant to R.A.C., NINDS R01 NS097161 to E.Ö., and NIGMS T32 GM007183 and NINDS FS31 NS120458 to M.L-R.

METHODS

Sequence selection and molecular cloning

cDNAs of most of the full-length Dprs and DIPs used in the study were obtained from Drosophila Genomics Research Center (DGRC). The remaining full-length sequences were generated through the extension of existing ectodomain constructs subcloned by our groups.[34] Among the DGRC clones, the sequence of Dpr15 required modification to remove the insertion within the Ig2 domain to preserve its structural integrity. The source, isoform, and identification number of each used sequence can be found in Table S1. Sequences of full-length Dprs and DIPs with an N-terminal V5 tag were cloned into the pMT/BiP/V5-His A vector (Invitrogen) for expression in S2 *Drosophila* cells for PLC cleavage assay or into the pAcGP67 baculovirus transfer vector (BD Biosciences) for expression in Sf9 cells for cell flow cytometry and cell aggregation

391 experiments. For cell aggregation, the constructs additionally included EGFP or
392 mScarlet separated from V5-tagged Dprs or DIPs by the P2A sequence.
393
394 **Predictions of GPI anchors and transmembrane helices**
395 Predictions of GPI-linkage were carried out using PredGPI[39] and NetGPI[40] tools
396 available online. For predictions using PredGPI the general model was used.
397 Predictions of transmembrane regions were performed using Phobius[36] and
398 DeepTMHMM[37]. Before analysis in Phobius and DeepTMHMM, the sequences of signal
399 peptides predicted with SignalP-6.0[38] were removed.
400
401 ***Drosophila* reagents, dissections, and immunohistochemistry**
402 All flies were kept at 25°C except when otherwise noted. Crosses were set at medium
403 density and crawling third instar larvae were dissected as before[49] in Phosphate
404 Buffered Saline (PBS, pH 7.4) on Sylgard dishes. Briefly, after fixing for 30 minutes in
405 4% paraformaldehyde, fillets were washed 3 times for 10 minutes in PBST (PBS +
406 0.05% Triton X-100, pH 7.4). Larval fillets were then blocked in 5% Normal Goat Serum
407 in PBST. Samples were incubated in primary antibodies diluted in block and overnight
408 at 4°C, extensively washed in PBST, and incubated with secondary antibodies for 2
409 hours at room temperature before the final washes in PBST. All washes and incubations
410 occurred on nutators. Samples were then mounted in Vectashield (Vector Laboratories)
411 and representative images were collected. HRP was used as a marker for neuronal
412 membranes and DLG was used as a marker for postsynaptic membranes.
413

The antibodies used for this study are:

Antibodies	Source	Concentration
Chicken anti-V5	Bethyl/A190-118A	1:200
Mouse anti-V5	Invitrogen R960-25	1:200
Rabbit anti-V5	Glotzer Lab	1:10,000
Rabbit anti-DLG	Budnik Lab	1:40,000
Mouse anti-α-Tubulin	Sigma DM1A	1:5,000
Goat anti-Mouse 488	Invitrogen A11029	1:500
Goat anti-Rabbit 488	Invitrogen A11008	1:500
Goat anti-Chicken 488	Invitrogen A11039	1:500
Goat anti-Rabbit 568	Invitrogen A11036	1:500
Goat anti-HRP 647	Jackson ImmunoResearch /123-605-021	1:100
Goat anti-Mouse 680	Jackson ImmunoResearch /115-625-146	1:5,000
Goat anti-Rabbit 790	Jackson ImmunoResearch /111-655-144	1:5,000

The fly lines used for this study are:

Genotype	Description	Source
W1118	White controls	BDSC
Mef2-GAL4	Muscle GAL4 driver	Ranganayakulu, et al., 1998[68]
A8-GAL4	Is neuron GAL4 driver	Wang, et al., 2021[52]
UAS-V5-Dpr19	V5 tagged Dpr19	This study
UAS-V5-Dpr10	V5 tagged Dpr10	Xu, et al., 2018[69]
UAS-Dpr10-CD4	First Ig domain from Dpr10, Ig5 and the TM from CD4	This study
UAS-CD4-Dpr10	First Ig from CD4, remainder of protein from Dpr10	This study
UAS-EGFP-DIP-ζ	sfGFP tagged DIP-ζ	This study
UAS-Myc-DIP-α	Myc tagged DIP-α (N)	This study
UAS-DIP-α-Myc	Myc tagged DIP-α (C)	Ashley, et al., 2019[23]
UAS-DIP-α-CD4	First Ig domain from DIP-α, Ig4+5 and the TM from CD4	This study

PLC cleavage assay with S2 cells

S2 cells were obtained from the Drosophila Genomics Research Center and maintained in Schneider's Medium (Sigma S0146), supplemented with Insect Media Supplement (Sigma I7267), and 90 U/ml Penicillin plus 90 µg/ml Streptomycin. Cells were maintained at room temperature. For experiments, confluent cells were split 1:2 into 6-well plates and transfected the following day. Complete Schneider's Media was mixed 2:1 with 250 µg/ml dimethyldioctadecyl-ammonium bromide (DDAB), allowed to mix, and then 500 µl DNA was added for each well to be transfected. Approximately 24 hours after transfection, protein expression was induced by adding 1 mM copper sulfate ($CuSO_4$). Three days later, 2 µl of 100 U/ml phosphatidylinositol-specific phospholipase C (PI-PLC, Life Technologies P-6466) was added to the treatment well, and cells were incubated for 4 hours.

To harvest cells, 2 ml from each well was collected and spun down at 500 x g for 5 minutes. The supernatant was collected and mixed with 6x Loading Buffer (375 mM Tris-Cl, pH 6.8, 9% SDS, 50% glycerol, 0.03% bromophenol blue, 9% β-mercaptoethanol) and boiled for 10 minutes. The cell pellet was washed in PBS and spun down as before. Next, cells were lysed used using a buffer adapted from Bumgarner et al., 2005,[70] consisting of 50 mM Tris-HCl pH 8.0, 150 mM NaCl, 1% Triton X-100, 5 mM EDTA, and protease inhibitors (one tablet per 50 ml; Pierce A32955). Tubes were incubated on a nutator at 4°C for 30 minutes and then at 37°C for 30 minutes. Tubes were centrifuged at 17,000 x g at room temperature for 15 minutes and mixed with 6x Loading Buffer.

Samples were then run on 12% SDS-polyacrylamide gels using the TGX FastCast system (BioRad 1610175). The samples were transferred overnight onto a nitrocellulose membrane (BioRad 1620115) at a constant current of 40 mA and blocked for one hour in 1% (w/v) Casein Block. Staining with primary and secondary antibodies was performed for 2 hours at room temperature with slight agitation and included washes in PBST after each incubation. Westerns were imaged on a LI-COR Odyssey imager.

Flow cytometry

Sf9 cell cultures at the density of 2×10^6 cells/ml were placed in 6-well plates, 3 ml per well. The cells were infected with baculoviruses encoding full-length Dprs and DIPs with an N-terminal V5 tag. Infected cultures were incubated for 48 hours on an orbital shaker at 125 rpm (Thermo MaxQ 430), at 28°C. 0.6 ml of each culture was transferred to a 24-well plate. 4 µl of PI-PLC per well was used for GPI cleavage. 4 µl of PI-PLC storage buffer (20 mM Tris-HCl, pH 7.5, 1 mM EDTA, 0.01% sodium azide, 50% glycerol) was added to control samples. Treatment was carried out for 3 hours on an orbital shaker at 125 rpm, at 28°C. Cultures were spun down for 1 minute at 500 x g. The cell pellets were resuspended in 300 µl of cold PBS, pH 7.4, with 1% BSA. 100 µl of cell suspensions were transferred to a U-shaped 96-well plate. 4 µl of anti-V5-AF647 antibody (R&D Systems, FAB8926R) was used for staining cells for 20 minutes on a shaker at 500 rpm (Thermo Microplate Shaker), at 4°C. Cultures were spun down for 1 minute at 500 x g, at 4°C and washed 3 times with 200 µl of PBS, pH 7.4, with 1% (w/v) BSA. Cells were analyzed using a BD Accuri C6 flow cytometer. 20,000 events were recorded per sample. The results were analyzed using FlowJo Software v10.8.1 (BD

Life Sciences).

Cell aggregation assay with Sf9 cells

Sf9 cultures at the density of 2×10^6 cells/ml were placed in 6-well plates, 3 ml per well, and infected with baculoviruses encoding (N- to C-terminal) mScarlet, P2A sequence (ATNFSLLKQAGDVEENPGP) and V5-tagged Dpr, or EGFP, P2A sequence, and V5-tagged DIP. This construct design was chosen to leave unmodified C-termini for Dprs and DIPs, as that would be important for testing for a C-terminal GPI anchoring signal. Infected cultures were incubated for 48 hours on an orbital shaker at 125 rpm, at 28°C. Expression of V5-tagged Dprs and DIPs was confirmed using western blots with the anti-V5-AF647 antibody. Cultures were diluted 1:15 in Sf9 complete media (Gibco Sf-900 III SFM, with 10% FBS, 2 mM L-glutamine, and 20 µg/ml gentamicin). 200 µl of cultures expressing Dprs were mixed with 200 µl of cultures expressing DIPs in 24-well plates. The control samples included 200 µl of cultures expressing individual Dprs or DIPs mixed with 200 µl of non-infected Sf9 cultures. Samples were prepared in triplicates for each Dpr–DIP pair and each control culture expressing individual Dprs and DIPs. Cultures were left to aggregate for 30 minutes on an orbital shaker at 125 rpm, at 28°C. 4 µl of PI-PLC per well was used for GPI cleavage. 4 µl of PI-PLC storage buffer was added to control samples. Treatment was carried out for 1 hour on an orbital shaker at 125 rpm, at 28°C. Cultures were imaged in 24-well plates at 5x magnification. Three images were collected for every well. Cell aggregation was quantified using the cell aggregation index, defined as the percentage of the total area occupied by cells that is comprised of aggregates.[71] The area occupied by cells and aggregates was

488 determined using the 'Analyze particles' function in Fiji. Aggregates were defined as
489 particles with areas of at least 2900 μm^2.
490
491 **Tissue PLC experiment**
492 Larvae were filleted, rinsed in PBS, and incubated while shaking for one hour in 1 ml of
493 PBS with or without 1 µl of PI-PLC. Larvae were washed with PBS, fixed, and stained
494 as above with a slight alteration: detergent was only used after staining for Dpr/DIP
495 protein tags. After extensive washing in PBS, anti-DLG was diluted in PBST and
496 incubated with larvae for 2 hours at room temperature. The subsequent washing and
497 secondary antibody staining was as described above. The staining procedure for PLC-
498 treated and untreated preparations was carried out in the same tube so that conditions
499 were identical. Three muscle 4 Ib arbors were imaged per animal.
500
501 For quantification, images were collected from each experiment using identical imaging
502 parameters. After measuring pixel sum of three terminal boutons per arbor, signal of the
503 Dpr/DIP was normalized to DLG signal to control for any differences in staining
504 conditions between replicates and because DLG should not be affected by PLC
505 treatment. These values are reported as 'Relative Pixel Sum' representing Tag/DLG
506 pixel sum.
507
508 **Tissue Localization experiment**
509 For localization experiments, crosses were maintained at 18°C in order to dampen
510 protein expression levels. Samples to be compared were pooled and stained as above,

omitting detergents in the first round of staining to label only proteins that were present on the cell surface at the time of fixation.

Once images were collected, z-stacks were generated, and the relevant channel was converted to 8-bit format before a threshold was set to convert image to binary representation of the surface protein stain. The same threshold was used for all images. This image was then used to count particles. For presynaptic localization, particles of and surrounding three terminal boutons per arbor were measured. For postsynaptic localization, particles of the entire image were counted. These manipulations were performed using ImageJ FIJI.[72]

Statistical Analysis

For tissue PLC experiments and tissue localization experiments, two-tailed Student's t-test was used to determine statistical significance (Prism 8). Cell aggregation experiments were evaluated using one-way ANOVA (Prism 9).

Tissue and cell imaging protocol

All in vivo images were obtained on a Zeiss LSM800 confocal microscope with a 40X plan-neofluar 1.3NA objective or 63X plan-apo 1.4NA objective. All images of Sf9 cells were obtained using a Leica THUNDER Imager 3D Cell Culture with Leica N Plan 5x/0.12 PH0 objective.

REFERENCES

1. Ferguson, M.A., and Williams, A.F. (1988). Cell-surface anchoring of proteins via glycosyl-phosphatidylinositol structures. Annu Rev Biochem *57*, 285–320. 10.1146/annurev.bi.57.070188.001441.

2. Low, M.G., and Finean, J.B. (1977). Non-lytic release of acetylcholinesterase from erythrocytes by a phosphatidylinositol-specific phospholipase C. FEBS Lett *82*, 143–146. 10.1016/0014-5793(77)80905-8.

3. Ikezawa, H., Yamanegi, M., Taguchi, R., Miyashita, T., and Ohyabu, T. (1976). Studies on phosphatidylinositol phosphodiesterase (phospholipase C type) of Bacillus cereus. I. purification, properties and phosphatase-releasing activity. Biochim Biophys Acta *450*, 154–164.

4. Eisenhaber, B., Bork, P., and Eisenhaber, F. (1999). Prediction of potential GPI-modification sites in proprotein sequences. J Mol Biol *292*, 741–758. 10.1006/jmbi.1999.3069.

5. Orlean, P., and Menon, A.K. (2007). Thematic review series: lipid posttranslational modifications. GPI anchoring of protein in yeast and mammalian cells, or: how we learned to stop worrying and love glycophospholipids. J Lipid Res *48*, 993–1011. 10.1194/jlr.R700002-JLR200.

6. UniProt Consortium (2015). UniProt: a hub for protein information. Nucleic Acids Res *43*, D204-212. 10.1093/nar/gku989.

7. Um, J.W., and Ko, J. (2017). Neural Glycosylphosphatidylinositol-Anchored Proteins in Synaptic Specification. Trends Cell Biol *27*, 931–945. 10.1016/j.tcb.2017.06.007.

8. Lukacs, M., Roberts, T., Chatuverdi, P., and Stottmann, R.W. (2019). Glycosylphosphatidylinositol biosynthesis and remodeling are required for neural tube closure, heart development, and cranial neural crest cell survival. Elife *8*, e45248. 10.7554/eLife.45248.

9. Wu, T., Yin, F., Guang, S., He, F., Yang, L., and Peng, J. (2020). The Glycosylphosphatidylinositol biosynthesis pathway in human diseases. Orphanet J Rare Dis *15*, 129. 10.1186/s13023-020-01401-z.

10. Kruger, R.P., Aurandt, J., and Guan, K.-L. (2005). Semaphorins command cells to move. Nat Rev Mol Cell Biol *6*, 789–800. 10.1038/nrm1740.

11. Pasterkamp, R.J., Peschon, J.J., Spriggs, M.K., and Kolodkin, A.L. (2003). Semaphorin 7A promotes axon outgrowth through integrins and MAPKs. Nature *424*, 398–405. 10.1038/nature01790.

12. Uesaka, N., Uchigashima, M., Mikuni, T., Nakazawa, T., Nakao, H., Hirai, H., Aiba, A., Watanabe, M., and Kano, M. (2014). Retrograde semaphorin signaling regulates synapse elimination in the developing mouse brain. Science *344*, 1020–1023. 10.1126/science.1252514.

13. Suzuki, K., Kumanogoh, A., and Kikutani, H. (2008). Semaphorins and their receptors in immune cell interactions. Nat Immunol *9*, 17–23. 10.1038/ni1553.

14. Eph Nomenclature Committee (1997). Unified nomenclature for Eph family receptors and their ligands, the Ephrins. Cell *90*, 403–404. 10.1016/s0092-8674(00)80500-0.

15. Gale, N.W., Holland, S.J., Valenzuela, D.M., Flenniken, A., Pan, L., Ryan, T.E., Henkemeyer, M., Strebhardt, K., Hirai, H., Wilkinson, D.G., et al. (1996). Eph receptors and ligands comprise two major specificity subclasses and are reciprocally compartmentalized during embryogenesis. Neuron *17*, 9–19. 10.1016/s0896-6273(00)80276-7.

16. Davy, A., Gale, N.W., Murray, E.W., Klinghoffer, R.A., Soriano, P., Feuerstein, C., and Robbins, S.M. (1999). Compartmentalized signaling by GPI-anchored ephrin-A5 requires the Fyn tyrosine kinase to regulate cellular adhesion. Genes Dev *13*, 3125–3135. 10.1101/gad.13.23.3125.

17. Hachisuka, A., Yamazaki, T., Sawada, J., and Terao, T. (1996). Characterization and tissue distribution of opioid-binding cell adhesion molecule (OBCAM) using monoclonal antibodies. Neurochem Int *28*, 373–379. 10.1016/0197-0186(95)00108-5.

18. Itoh, S., Hachisuka, A., Kawasaki, N., Hashii, N., Teshima, R., Hayakawa, T., Kawanishi, T., and Yamaguchi, T. (2008). Glycosylation analysis of IgLON family proteins in rat brain by liquid chromatography and multiple-stage mass spectrometry. Biochemistry *47*, 10132–10154. 10.1021/bi8009778.

19. Sanz, R., Ferraro, G.B., and Fournier, A.E. (2015). IgLON cell adhesion molecules are shed from the cell surface of cortical neurons to promote neuronal growth. J Biol Chem *290*, 4330–4342. 10.1074/jbc.M114.628438.

20. Struyk, A.F., Canoll, P.D., Wolfgang, M.J., Rosen, C.L., D'Eustachio, P., and Salzer, J.L. (1995). Cloning of neurotrimin defines a new subfamily of differentially expressed neural cell adhesion molecules. J Neurosci *15*, 2141–2156. 10.1523/JNEUROSCI.15-03-02141.1995.

21. Pischedda, F., and Piccoli, G. (2016). The IgLON Family Member Negr1 Promotes Neuronal Arborization Acting as Soluble Factor via FGFR2. Front Mol Neurosci *8*, 89. 10.3389/fnmol.2015.00089.

22. Cheng, S., Park, Y., Kurleto, J.D., Jeon, M., Zinn, K., Thornton, J.W., and Özkan, E. (2019). Family of neural wiring receptors in bilaterians defined by phylogenetic, biochemical, and structural evidence. Proc Natl Acad Sci U S A *116*, 9837–9842. 10.1073/pnas.1818631116.

23. Ashley, J., Sorrentino, V., Lobb-Rabe, M., Nagarkar-Jaiswal, S., Tan, L., Xu, S., Xiao, Q., Zinn, K., and Carrillo, R.A. (2019). Transsynaptic interactions between IgSF proteins DIP-α and Dpr10 are required for motor neuron targeting specificity. eLife *8*, e42690. 10.7554/eLife.42690.

24. Carrillo, R.A., Özkan, E., Menon, K.P., Nagarkar-Jaiswal, S., Lee, P.-T., Jeon, M., Birnbaum, M.E., Bellen, H.J., Garcia, K.C., and Zinn, K. (2015). Control of Synaptic Connectivity by a Network of Drosophila IgSF Cell Surface Proteins. Cell *163*, 1770–1782. 10.1016/j.cell.2015.11.022.

25. Courgeon, M., and Desplan, C. (2019). Coordination between stochastic and deterministic specification in the Drosophila visual system. Science *366*, eaay6727. 10.1126/science.aay6727.

26. Menon, K.P., Kulkarni, V., Takemura, S.-Y., Anaya, M., and Zinn, K. (2019). Interactions between Dpr11 and DIP-γ control selection of amacrine neurons in Drosophila color vision circuits. eLife *8*, e48935. 10.7554/eLife.48935.

27. Venkatasubramanian, L., Guo, Z., Xu, S., Tan, L., Xiao, Q., Nagarkar-Jaiswal, S., and Mann, R.S. (2019). Stereotyped terminal axon branching of leg motor neurons mediated by IgSF proteins DIP-α and Dpr10. eLife *8*, e42692. 10.7554/eLife.42692.

28. Xu, C., Theisen, E., Maloney, R., Peng, J., Santiago, I., Yapp, C., Werkhoven, Z., Rumbaut, E., Shum, B., Tarnogorska, D., et al. (2019). Control of Synaptic Specificity by Establishing a Relative Preference for Synaptic Partners. Neuron *103*, 865-877.e7. 10.1016/j.neuron.2019.06.006.

29. Barish, S., Nuss, S., Strunilin, I., Bao, S., Mukherjee, S., Jones, C.D., and Volkan, P.C. (2018). Combinations of DIPs and Dprs control organization of olfactory receptor neuron terminals in Drosophila. PLoS Genet *14*, e1007560. 10.1371/journal.pgen.1007560.

30. Bornstein, B., Meltzer, H., Adler, R., Alyagor, I., Berkun, V., Cummings, G., Reh, F., Keren-Shaul, H., David, E., Riemensperger, T., et al. (2021). Transneuronal Dpr12/DIP-δ interactions facilitate compartmentalized dopaminergic innervation of Drosophila mushroom body axons. EMBO J *40*, e105763. 10.15252/embj.2020105763.

31. Lobb-Rabe, M., DeLong, K., Salazar, R.J., Zhang, R., Wang, Y., and Carrillo, R.A. (2022). Dpr10 and Nocte are required for Drosophila motor axon pathfinding. Neural Dev *17*, 10. 10.1186/s13064-022-00165-5.

32. Xu, S., Sergeeva, A.P., Katsamba, P.S., Mannepalli, S., Bahna, F., Bimela, J., Zipursky, S.L., Shapiro, L., Honig, B., and Zinn, K. (2022). Affinity requirements for control of synaptic targeting and neuronal cell survival by heterophilic IgSF cell adhesion molecules. Cell Rep *39*, 110618. 10.1016/j.celrep.2022.110618.

33. Brovero, S.G., Fortier, J.C., Hu, H., Lovejoy, P.C., Newell, N.R., Palmateer, C.M., Tzeng, R.-Y., Lee, P.-T., Zinn, K., and Arbeitman, M.N. (2021). Investigation of Drosophila fruitless neurons that express Dpr/DIP cell adhesion molecules. eLife *10*, e63101. 10.7554/eLife.63101.

34. Özkan, E., Carrillo, R.A., Eastman, C.L., Weiszmann, R., Waghray, D., Johnson, K.G., Zinn, K., Celniker, S.E., and Garcia, K.C. (2013). An Extracellular Interactome of Immunoglobulin and LRR Proteins Reveals Receptor-Ligand Networks. Cell *154*, 228–239. 10.1016/j.cell.2013.06.006.

35. Ranaivoson, F.M., Turk, L.S., Ozgul, S., Kakehi, S., von Daake, S., Lopez, N., Trobiani, L., De Jaco, A., Denissova, N., Demeler, B., et al. (2019). A Proteomic Screen of Neuronal Cell-Surface Molecules Reveals IgLONs as Structurally Conserved Interaction Modules at the Synapse. Structure *27*, 893-906.e9. 10.1016/j.str.2019.03.004.

36. Käll, L., Krogh, A., and Sonnhammer, E.L.L. (2004). A combined transmembrane topology and signal peptide prediction method. J Mol Biol *338*, 1027–1036. 10.1016/j.jmb.2004.03.016.

37. Hallgren, J., Tsirigos, K.D., Pedersen, M.D., Armenteros, J.J.A., Marcatili, P., Nielsen, H., Krogh, A., and Winther, O. (2022). DeepTMHMM predicts alpha and beta transmembrane proteins using deep neural networks. 2022.04.08.487609. 10.1101/2022.04.08.487609.

38. Teufel, F., Almagro Armenteros, J.J., Johansen, A.R., Gíslason, M.H., Pihl, S.I., Tsirigos, K.D., Winther, O., Brunak, S., von Heijne, G., and Nielsen, H. (2022). SignalP 6.0 predicts all five types of signal peptides using protein language models. Nat Biotechnol *40*, 1023–1025. 10.1038/s41587-021-01156-3.

39. Pierleoni, A., Martelli, P.L., and Casadio, R. (2008). PredGPI: a GPI-anchor predictor. BMC Bioinformatics *9*, 392. 10.1186/1471-2105-9-392.

40. Gíslason, M.H., Nielsen, H., Almagro Armenteros, J.J., and Johansen, A.R. (2021). Prediction of GPI-anchored proteins with pointer neural networks. Curr Res Biotechnol *3*, 6–13. 10.1016/j.crbiot.2021.01.001.

41. Butler, S.J., Ray, S., and Hiromi, Y. (1997). klingon, a novel member of the Drosophila immunoglobulin superfamily, is required for the development of the R7 photoreceptor neuron. Development *124*, 781–792. 10.1242/dev.124.4.781.

42. Ramos, R.G., Igloi, G.L., Lichte, B., Baumann, U., Maier, D., Schneider, T., Brandstätter, J.H., Fröhlich, A., and Fischbach, K.F. (1993). The irregular chiasm C-roughest locus of Drosophila, which affects axonal projections and programmed cell death, encodes a novel immunoglobulin-like protein. Genes Dev *7*, 2533–2547. 10.1101/gad.7.12b.2533.

43. Ruiz-Gómez, M., Coutts, N., Price, A., Taylor, M.V., and Bate, M. (2000). Drosophila dumbfounded: a myoblast attractant essential for fusion. Cell *102*, 189–198. 10.1016/s0092-8674(00)00024-6.

44. Honig, B., and Shapiro, L. (2020). Adhesion Protein Structure, Molecular Affinities, and Principles of Cell-Cell Recognition. Cell *181*, 520–535. 10.1016/j.cell.2020.04.010.

45. Kumari, S.S., and Varadaraj, K. (2009). Intact AQP0 performs cell-to-cell adhesion. Biochem Biophys Res Commun *390*, 1034–1039. 10.1016/j.bbrc.2009.10.103.

46. Yoshida, C., and Takeichi, M. (1982). Teratocarcinoma cell adhesion: identification of a cell-surface protein involved in calcium-dependent cell aggregation. Cell *28*, 217–224. 10.1016/0092-8674(82)90339-7.

47. Cosmanescu, F., Katsamba, P.S., Sergeeva, A.P., Ahlsen, G., Patel, S.D., Brewer, J.J., Tan, L., Xu, S., Xiao, Q., Nagarkar-Jaiswal, S., et al. (2018). Neuron-Subtype-Specific Expression, Interaction Affinities, and Specificity Determinants of DIP/Dpr Cell Recognition Proteins. Neuron *100*, 1385-1400.e6. 10.1016/j.neuron.2018.10.046.

48. Cheng, S., Ashley, J., Kurleto, J.D., Lobb-Rabe, M., Park, Y.J., Carrillo, R.A., and Özkan, E. (2019). Molecular basis of synaptic specificity by immunoglobulin superfamily receptors in Drosophila. eLife *8*, e41028. 10.7554/eLife.41028.

49. Wang, Y., Lobb-Rabe, M., Ashley, J., Chatterjee, P., Anand, V., Bellen, H.J., Kanca, O., and Carrillo, R.A. (2022). Systematic expression profiling of Dpr and DIP genes reveals cell surface codes in Drosophila larval motor and sensory neurons. Development *149*, dev200355. 10.1242/dev.200355.

50. Arumugam, S., Schmieder, S., Pezeshkian, W., Becken, U., Wunder, C., Chinnapen, D., Ipsen, J.H., Kenworthy, A.K., Lencer, W., Mayor, S., et al. (2021). Ceramide structure dictates glycosphingolipid nanodomain assembly and function. Nat Commun *12*, 3675. 10.1038/s41467-021-23961-9.

51. Sharma, P., Varma, R., Sarasij, R.C., Ira, Gousset, K., Krishnamoorthy, G., Rao, M., and Mayor, S. (2004). Nanoscale organization of multiple GPI-anchored proteins in living cell membranes. Cell *116*, 577–589. 10.1016/s0092-8674(04)00167-9.

52. Wang, Y., Lobb-Rabe, M., Ashley, J., Anand, V., and Carrillo, R.A. (2021). Structural and Functional Synaptic Plasticity Induced by Convergent Synapse Loss in the Drosophila Neuromuscular Circuit. J Neurosci *41*, 1401–1417. 10.1523/JNEUROSCI.1492-20.2020.

53. Levental, I., Levental, K.R., and Heberle, F.A. (2020). Lipid Rafts: Controversies Resolved, Mysteries Remain. Trends Cell Biol *30*, 341–353. 10.1016/j.tcb.2020.01.009.

54. Kato, M., Wang, H., Kainulainen, V., Fitzgerald, M.L., Ledbetter, S., Ornitz, D.M., and Bernfield, M. (1998). Physiological degradation converts the soluble syndecan-1 ectodomain from an inhibitor to a potent activator of FGF-2. Nat Med *4*, 691–697. 10.1038/nm0698-691.

55. Reiss, K., Maretzky, T., Ludwig, A., Tousseyn, T., de Strooper, B., Hartmann, D., and Saftig, P. (2005). ADAM10 cleavage of N-cadherin and regulation of cell-cell adhesion and beta-catenin nuclear signalling. EMBO J *24*, 742–752. 10.1038/sj.emboj.7600548.

56. Lee, G.-H., Fujita, M., Takaoka, K., Murakami, Y., Fujihara, Y., Kanzawa, N., Murakami, K.-I., Kajikawa, E., Takada, Y., Saito, K., et al. (2016). A GPI processing phospholipase A2, PGAP6, modulates Nodal signaling in embryos by shedding CRIPTO. J Cell Biol *215*, 705–718. 10.1083/jcb.201605121.

57. Dyczynska, E., Sun, D., Yi, H., Sehara-Fujisawa, A., Blobel, C.P., and Zolkiewska, A. (2007). Proteolytic processing of delta-like 1 by ADAM proteases. J Biol Chem *282*, 436–444. 10.1074/jbc.M605451200.

58. Mishra-Gorur, K., Rand, M.D., Perez-Villamil, B., and Artavanis-Tsakonas, S. (2002). Down-regulation of Delta by proteolytic processing. J Cell Biol *159*, 313–324. 10.1083/jcb.200203117.

59. Boyer-Di Ponio, J., Wright-Crosnier, C., Groyer-Picard, M.-T., Driancourt, C., Beau, I., Hadchouel, M., and Meunier-Rotival, M. (2007). Biological function of mutant forms of JAGGED1 proteins in Alagille syndrome: inhibitory effect on Notch signaling. Hum Mol Genet *16*, 2683–2692. 10.1093/hmg/ddm222.

60. Steinbuck, M.P., and Winandy, S. (2018). A Review of Notch Processing With New Insights Into Ligand-Independent Notch Signaling in T-Cells. Front Immunol *9*, 1230. 10.3389/fimmu.2018.01230.

61. Droujinine, I.A., Meyer, A.S., Wang, D., Udeshi, N.D., Hu, Y., Rocco, D., McMahon, J.A., Yang, R., Guo, J., Mu, L., et al. (2021). Proteomics of protein trafficking by in vivo tissue-specific labeling. Nat Commun *12*, 2382. 10.1038/s41467-021-22599-x.

62. Peixoto, R.T., Kunz, P.A., Kwon, H., Mabb, A.M., Sabatini, B.L., Philpot, B.D., and Ehlers, M.D. (2012). Transsynaptic signaling by activity-dependent cleavage of neuroligin-1. Neuron *76*, 396–409. 10.1016/j.neuron.2012.07.006.

63. Rodríguez-Manzaneque, J.C., Carpizo, D., Plaza-Calonge, M. del C., Torres-Collado, A.X., Thai, S.N.-M., Simons, M., Horowitz, A., and Iruela-Arispe, M.L. (2009). Cleavage of syndecan-4 by ADAMTS1 provokes defects in adhesion. Int J Biochem Cell Biol *41*, 800–810. 10.1016/j.biocel.2008.08.014.

64. Stahl, R., Schilling, S., Soba, P., Rupp, C., Hartmann, T., Wagner, K., Merdes, G., Eggert, S., and Kins, S. (2014). Shedding of APP limits its synaptogenic activity and cell adhesion properties. Front Cell Neurosci *8*, 410. 10.3389/fncel.2014.00410.

65. Suzuki, K., Hayashi, Y., Nakahara, S., Kumazaki, H., Prox, J., Horiuchi, K., Zeng, M., Tanimura, S., Nishiyama, Y., Osawa, S., et al. (2012). Activity-dependent proteolytic cleavage of neuroligin-1. Neuron *76*, 410–422. 10.1016/j.neuron.2012.10.003.

66. Toth, A.B., Terauchi, A., Zhang, L.Y., Johnson-Venkatesh, E.M., Larsen, D.J., Sutton, M.A., and Umemori, H. (2013). Synapse maturation by activity-dependent ectodomain shedding of SIRPα. Nat Neurosci *16*, 1417–1425. 10.1038/nn.3516.

67. Corda, D., Mosca, M.G., Ohshima, N., Grauso, L., Yanaka, N., and Mariggiò, S. (2014). The emerging physiological roles of the glycerophosphodiesterase family. FEBS J *281*, 998–1016. 10.1111/febs.12699.

68. Ranganayakulu, G., Elliott, D.A., Harvey, R.P., and Olson, E.N. (1998). Divergent roles for NK-2 class homeobox genes in cardiogenesis in flies and mice. Development *125*, 3037–3048. 10.1242/dev.125.16.3037.

69. Xu, S., Xiao, Q., Cosmanescu, F., Sergeeva, A.P., Yoo, J., Lin, Y., Katsamba, P.S., Ahlsen, G., Kaufman, J., Linaval, N.T., et al. (2018). Interactions between the Ig-Superfamily Proteins DIP-α and Dpr6/10 Regulate Assembly of Neural Circuits. Neuron *100*, 1369-1384.e6. 10.1016/j.neuron.2018.11.001.

70. Bumgarner, G.W., Zampell, J.C., Nagarajan, S., Poloso, N.J., Dorn, A.S., D'Souza, M.J., and Selvaraj, P. (2005). Modified cell ELISA to determine the solubilization of cell surface proteins: Applications in GPI-anchored protein purification. J Biochem Biophys Methods *64*, 99–109. 10.1016/j.jbbm.2005.05.007.

71. Boucard, A.A., Ko, J., and Südhof, T.C. (2012). High affinity neurexin binding to cell adhesion G-protein-coupled receptor CIRL1/latrophilin-1 produces an intercellular adhesion complex. J Biol Chem *287*, 9399–9413. 10.1074/jbc.M111.318659.

72. Schindelin, J., Arganda-Carreras, I., Frise, E., Kaynig, V., Longair, M., Pietzsch, T., Preibisch, S., Rueden, C., Saalfeld, S., Schmid, B., et al. (2012). Fiji: an open-source platform for biological-image analysis. Nat Methods *9*, 676–682. 10.1038/nmeth.2019.

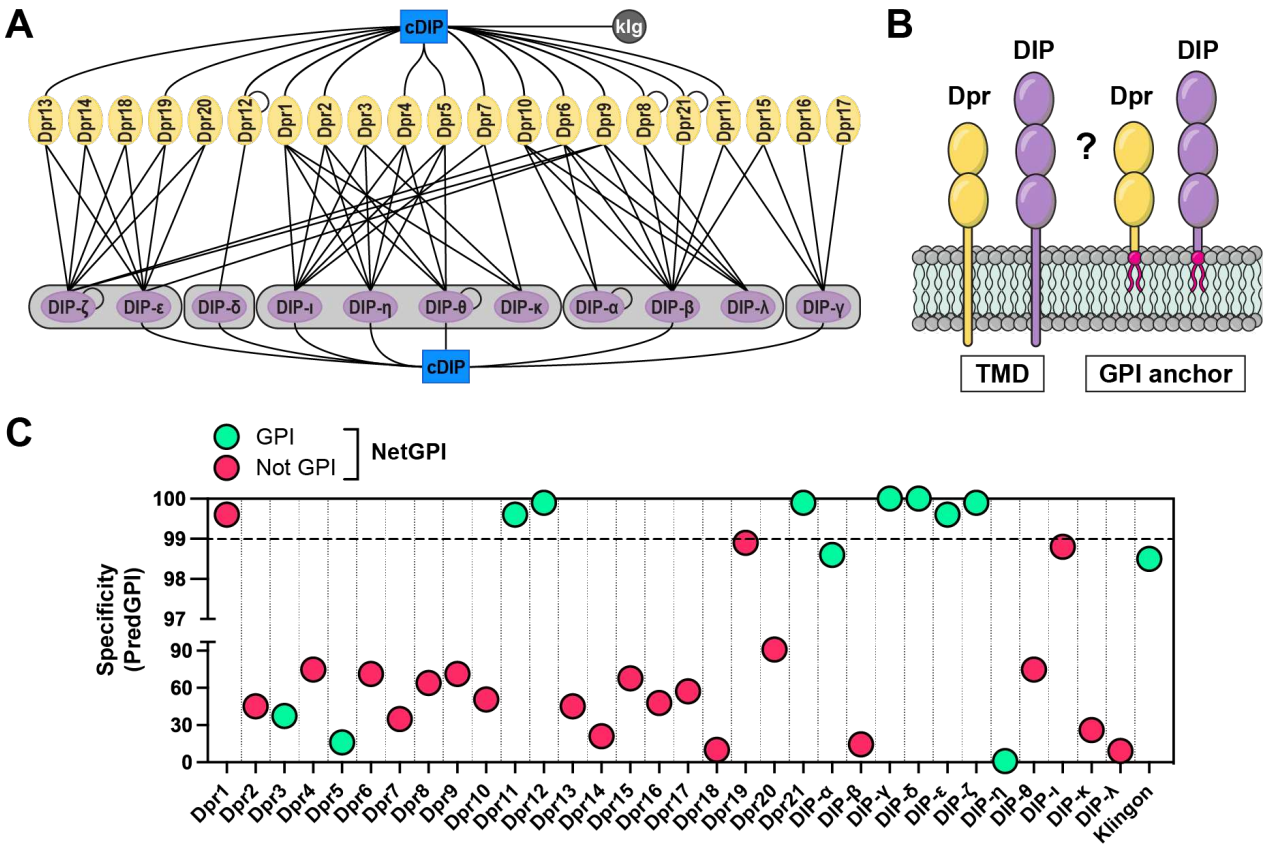

Figure 1. GPI anchoring predictions for the Dpr and DIP families of CSPs. (A) Dpr-DIP interactome. Lines indicate interactions determined in previously published *in vitro* studies. cDIP, common DIP-interacting protein; Klg, Klingon. (B) Two potential membrane-anchoring modes of Dprs and DIPs. TMD, transmembrane domain; GPI, glycosylphosphatidylinositol. (C) GPI anchor predictions using PredGPI and NetGPI. Specificity values as calculated by PredGPI were plotted for each protein. Proteins with specificity values above 99% are considered GPI-anchored. For NetGPI, positive predictions are shown as green and negative are shown as red.

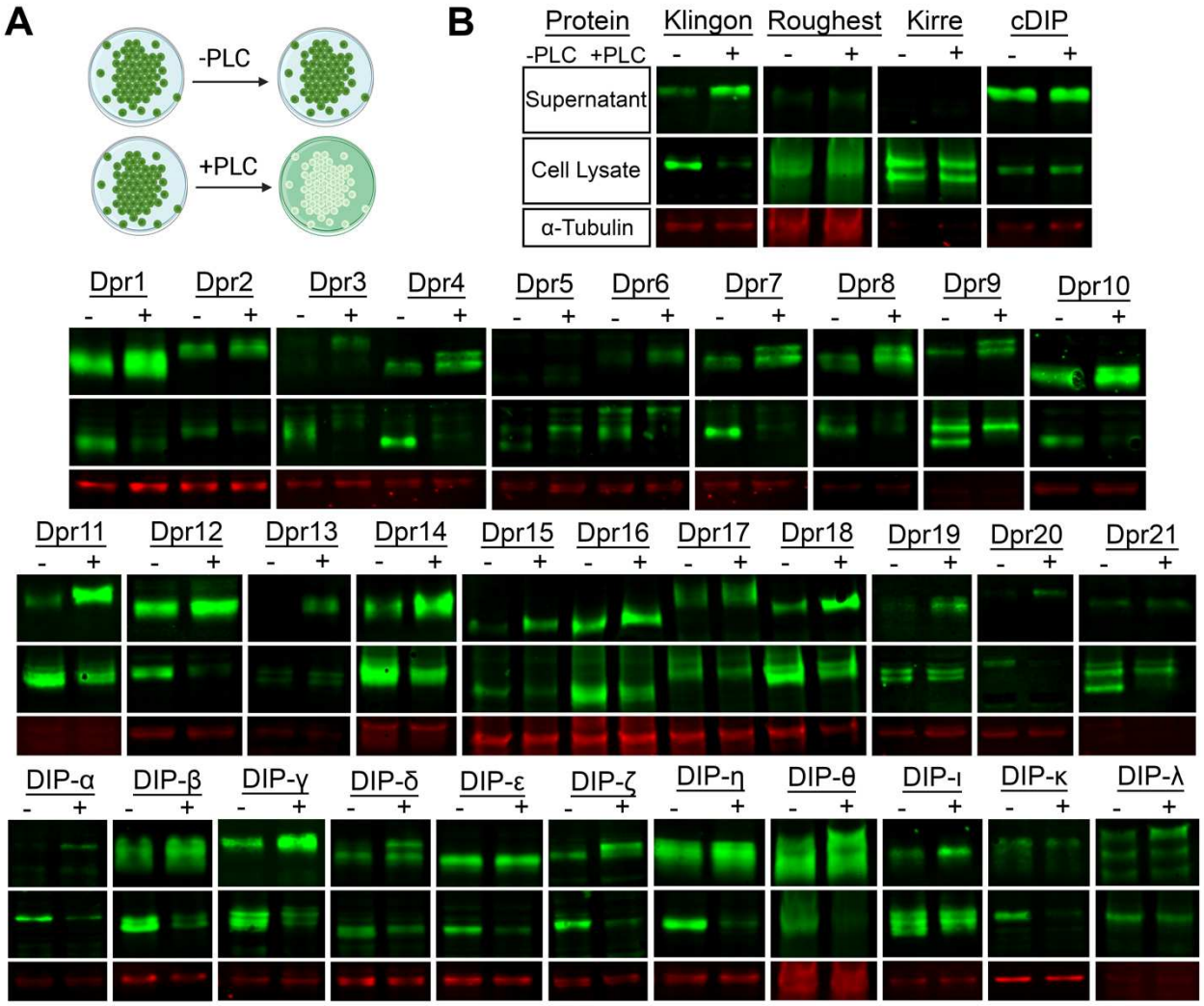

Figure 2. PLC treatment cleaves Dprs and DIPs from S2 cells, as observed by western blotting. (A) Schematic for PLC cleavage assay on S2 cells, when a CSP is GPI anchored. Green color indicates where the GPI-anchored protein is (on cells or in culture media). (B) Western blots of the supernatant fraction, cell lysate, and Tubulin-α loading control for with (+) and without (–) PLC treatment for all members of Dpr/DIP subfamilies. See key in the top row for B.

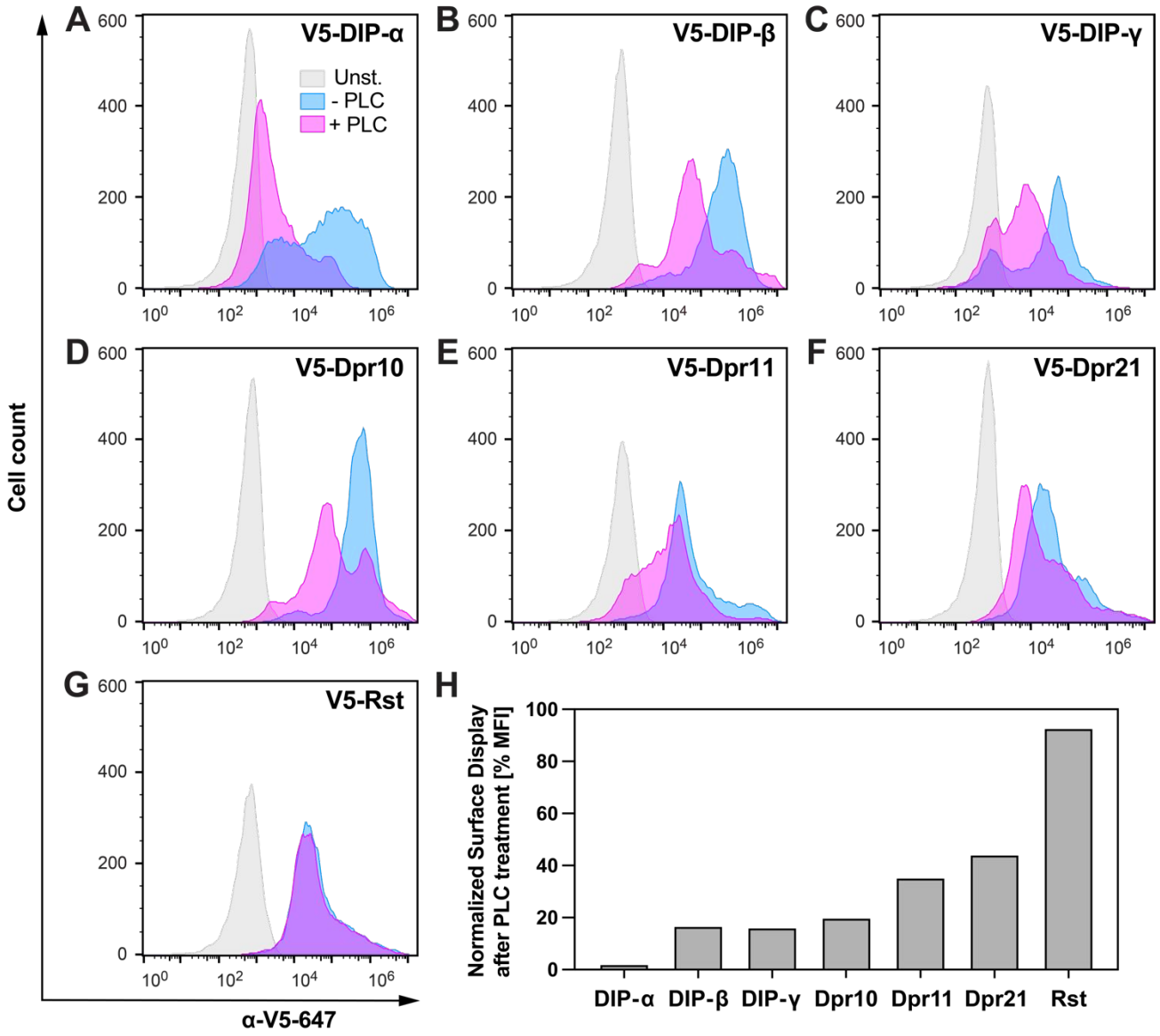

Figure 3. Surface display of Dprs and DIPs is reduced by PLC treatment, as observed by flow cytometry. (A-G) Histograms showing fluorescence levels of baculovirus-infected, unstained Sf9 cells (gray), cells infected and stained with anti-V5-Alexa Fluor 647 antibody (blue), and cells infected, treated with PLC and stained with anti-V5-Alexa Fluor 647 antibody (magenta). (H) Remaining Dpr and DIP levels on Sf9 cell surface following PLC treatment, normalized as the ratio of median fluorescence intensity (MFI) for PLC-treated and not treated cells after subtraction of the background MFI value of unstained cells.

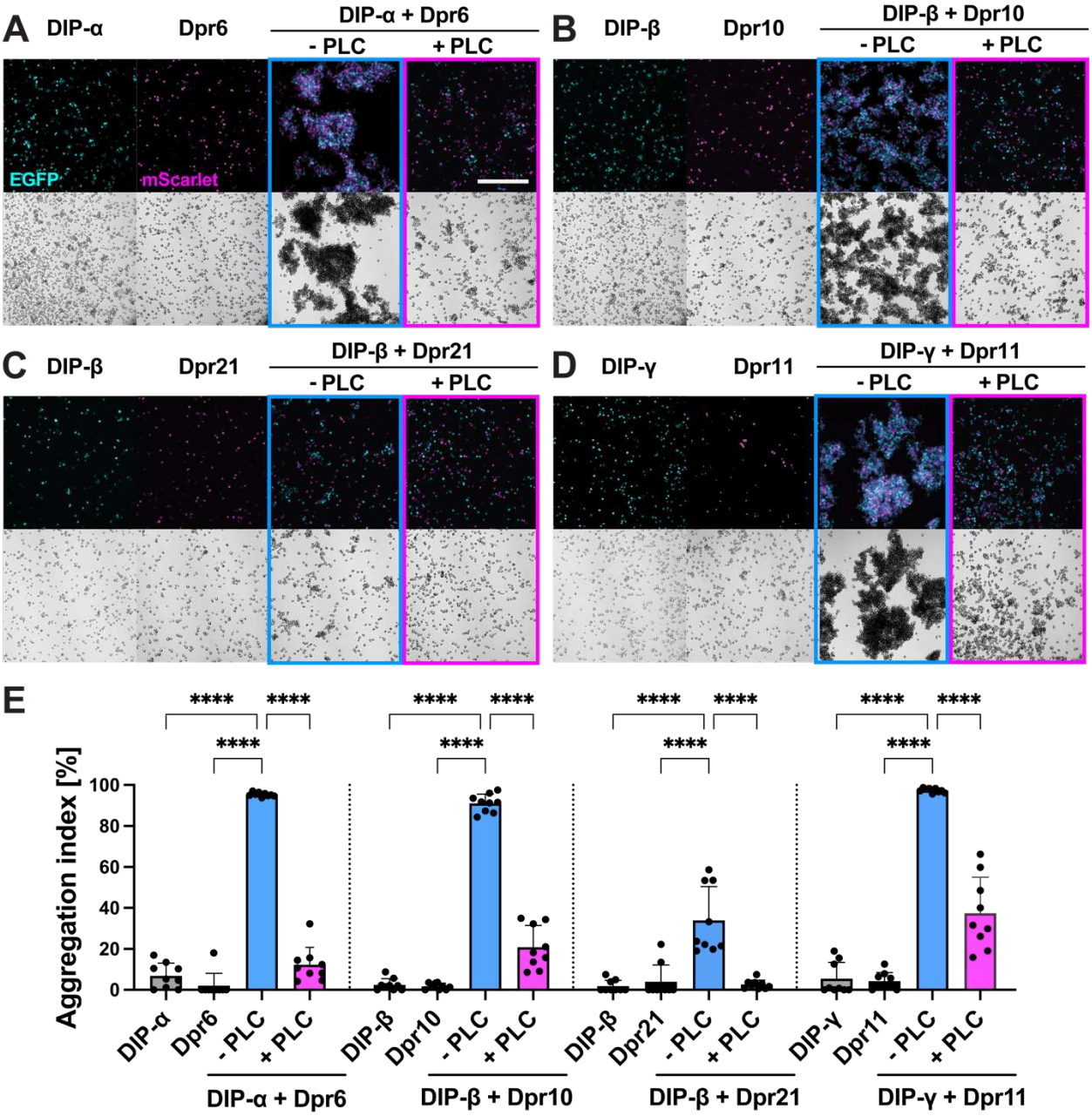

Figure 4. PLC cleavage eliminates Dpr–DIP-mediated cell aggregation. (A-D) Cell aggregation experiments with Sf9 cells. Controls included cultures expressing either DIP or Dpr (first two panels from the left) and cultures expressing DIP or Dpr mixed together but not treated with PLC (-PLC). Cell aggregation was abolished when PLC was added to the mixed cultures 30 minutes after aggregation (+PLC). Scale bar = 500 μm. (E) Cell aggregation index for the samples shown in A-D; ****p<0.0001; one-way ANOVA.

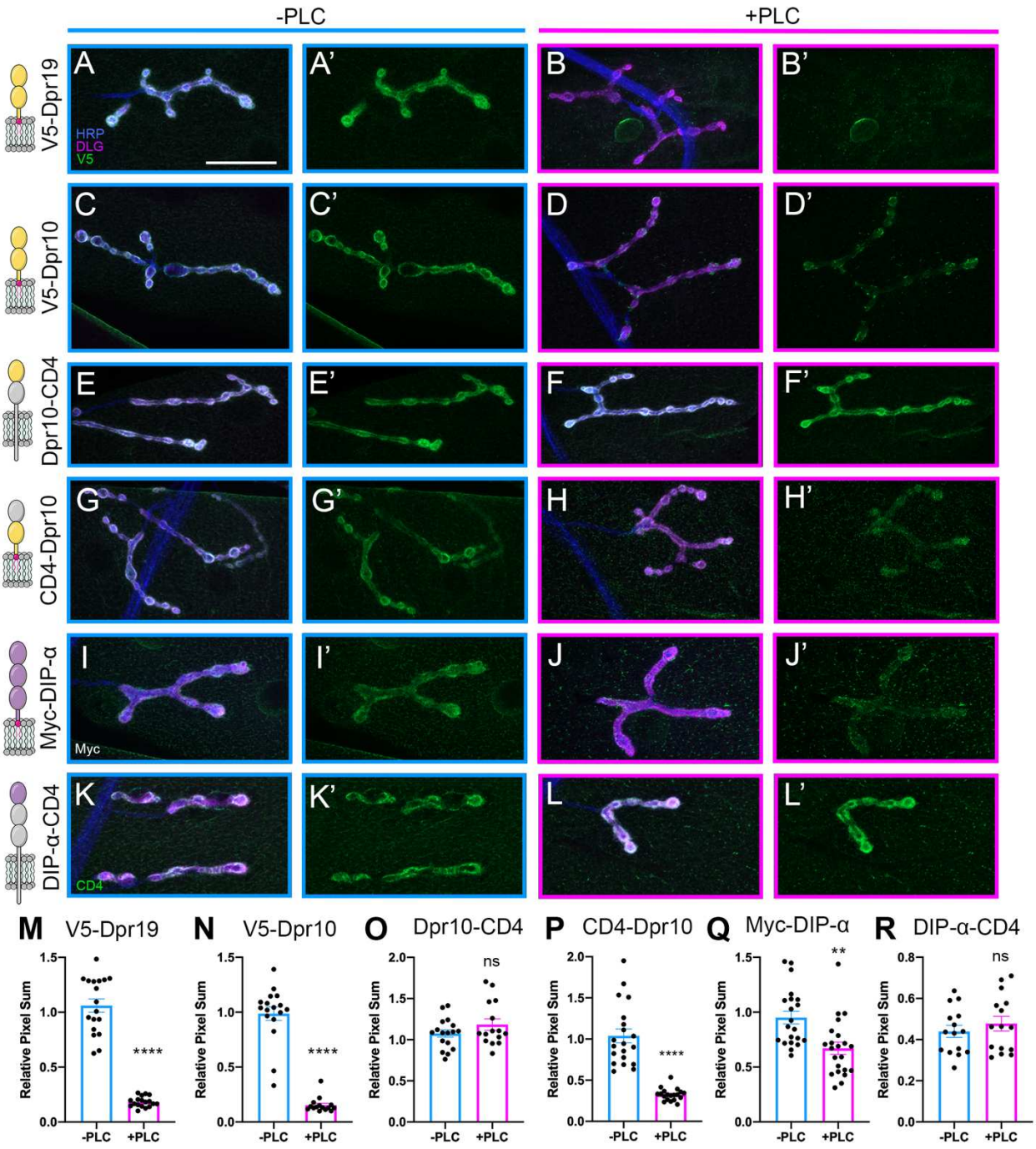

Figure 5. Dpr and DIP proteins are GPI anchored in vivo. (A-L') Tagged Dprs and DIPs were expressed in muscles, and dissected larvae were treated with PLC and compared to non-treated controls. Cartoon presentations of tagged Dprs and DIPs and their domains are depicted in left column. Surface localized proteins are shown in green, neuronal tissue in blue (HRP), and postsynaptic membrane in magenta (DLG). (A-B) PLC efficiently reduced surface labeling of V5 on muscles expressing V5-Dpr19. (C-D) PLC efficiently reduced surface labeling of V5 on muscles expressing V5-Dpr19. (E-F) PLC failed to reduce labeling of V5 in muscles expressing Dpr10-CD4 chimeras. (G-H) PLC efficiently reduced surface labeling of V5 in muscles expressing CD4-Dpr10 chimeras. (I-J) PLC reduced surface labeling of Myc on muscles expressing Myc-DIP-α. (K-L) PLC failed to reduce muscle labeling of CD4 on muscles expressing DIP-α-CD4 chimeras (M-R) Quantification of experiments shown in A-L'. Scale bar = 50 μm.

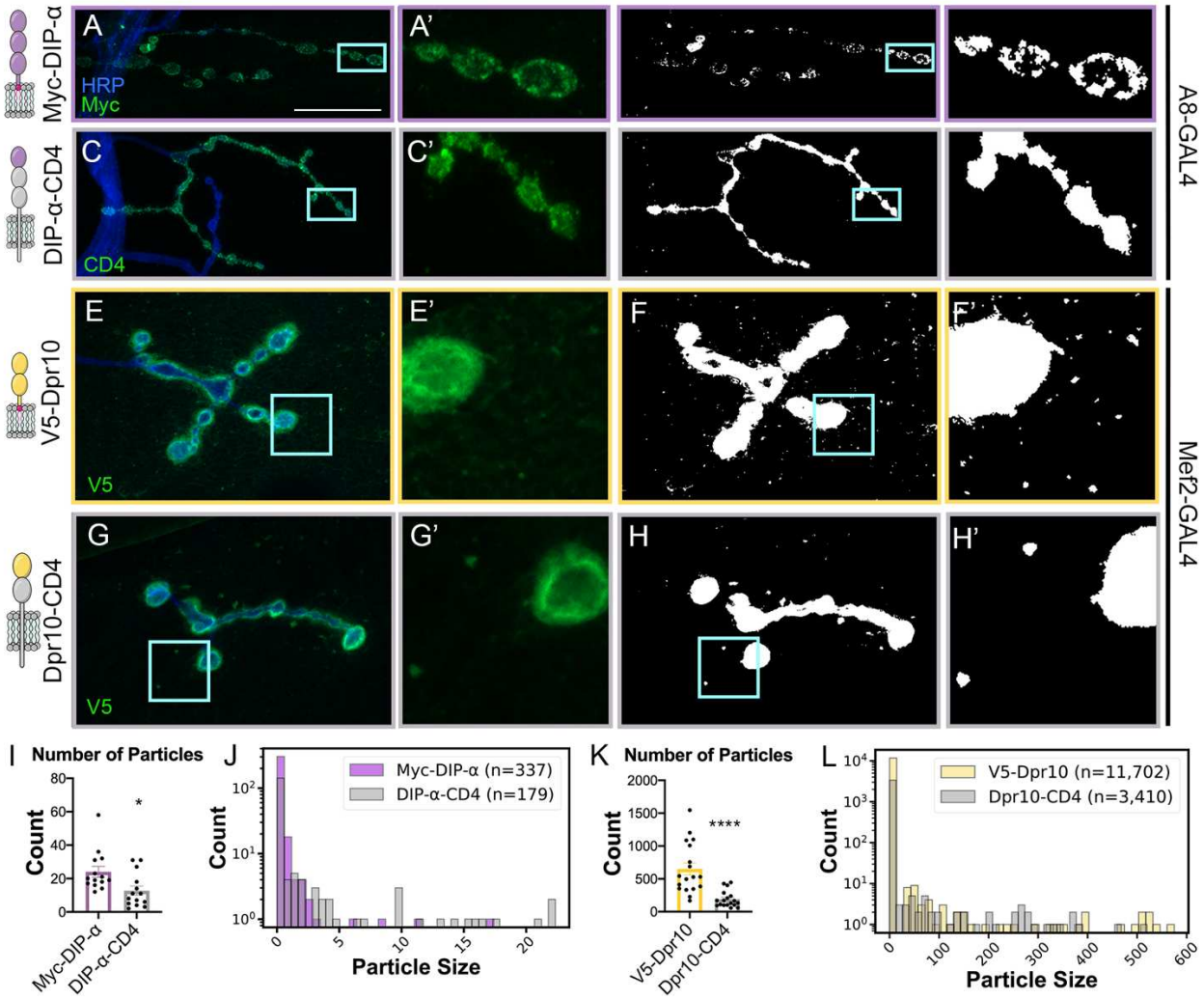

Figure 6. GPI anchor alters localization of DIP-α in neurons and Dpr10 in muscles. (A-H') Cartoon depictions of constructs are shown in left column. Surface localized proteins are shown in green, neuronal tissue in blue (HRP). Scale bar = 50 μm. (A-B) Tagged DIP-α and DIP-α-CD4 were expressed in Is motor neurons. (A-A') *A8-GAL4* driving Myc-DIP-α leads to punctate surface localization outside the boutons. (B-B') Binary thresholded image of A. (C-C') *A8-GAL4* driving DIP-α-CD4 leads to localization of DIP-α throughout the Is motor neuron terminal. (D-D') Binary thresholded image of C. (E-E') *Mef2-GAL4* driving V5-Dpr10 leads to punctate surface localization. (F-F') Binary thresholded image of E. (G-G') *Mef2-GAL4* driving Dpr10-CD4 leads to loss of Dpr10 throughout the muscle surface. (H-H') Binary thresholded image of G. (I,K) Particles counted for experiments depicted in A-D and E-H, respectively. (J, L) Histogram showing counts for particle size distribution.

SUPPLEMENTAL MATERIALS

Table S1. Selection of sequences used in our analyses. X under isoform indicates the exact sequence for the predicted isoform does not exist in Flybase.

Protein	Isoform	FlyBase ID	Source	DGRC cDNA clone
Dpr1	A	FBcl0481435	DGRC	IP20514
Dpr2	F	FBtr0340553	Extended ECD	-
Dpr3	B	FBtr0300671	Extended ECD	-
Dpr4	B	FBcl0702669	DGRC	FI04761
Dpr5	B	FBcl0135155	DGRC	GH08163
Dpr6	C	FBtr0331536	Extended ECD	-
Dpr7	F	FBtr0334408	Extended ECD	-
Dpr8	A	FBcl0120305	DGRC	GH05565
Dpr9	X	FBcl0129707	DGRC	GH01517
Dpr10	D	FBtr0331552	Extended ECD	-
Dpr11	B	FBcl0127201	DGRC	GH22307
Dpr12	C	FBcl0317539	DGRC	IP17045
Dpr13	B	FBcl0345923	DGRC	IP04317
Dpr14	A	FBcl0119149	DGRC	GH19181
Dpr15	X	FBcl0474633	DGRC	FI05813
Dpr16	B	FBtr0110950	Extended ECD	-
Dpr17	A	FBcl0743266	DGRC	FI20195
Dpr18	A	FBcl0212563	DGRC	RE24718
Dpr19	A	FBcl0191639	DGRC	LP09705
Dpr20	A	FBcl0124577	DGRC	GH16485
Dpr21	C	FBtr0334939	Extended ECD	-
DIP-α	A	FBcl0222778	DGRC	RE16159
DIP-β	G	FBtr0343091	Extended ECD	-
DIP-γ	A	FBcl0116341	DGRC	GH08175
DIP-δ	D	FBcl0303889	DGRC	IP08460
DIP-ε	A	FBtr0299967	Extended ECD	-
DIP-ζ	A	FBcl0474748	DGRC	FI03417
DIP-η	B	FBtr0302933	Extended ECD	-
DIP-θ	A	FBtr0079114	Extended ECD	-
DIP-ι	B	FBcl0293758	DGRC	IP10422
DIP-κ	A	FBcl0202207	DGRC	RE42927
DIP-λ	A	FBtr0346766	Extended ECD	-
Klingon	-	FBcl0158367	DGRC	LD10776

Table S2. GPI site predictions by PredGPI and NetGPI. Results of GPI-anchor site predictions with PredGPI and NetGPI. Values of specificity index calculated by PredGPI indicate the probability of the presence of a GPI-anchor. Likelihood values for the positive calls from NetGPI pertain to the prediction of the ω site position.

Protein	PredGPI prediction	Specificity	NetGPI prediction	Likelihood
Dpr1	GPI	99.60%	Not-GPI	0.975
Dpr2	Not-GPI	45.20%	Not-GPI	0.978
Dpr3	Not-GPI	37.30%	GPI	0.565
Dpr4	Not-GPI	74.80%	Not-GPI	0.813
Dpr5	Not-GPI	16.00%	GPI	0.407
Dpr6	Not-GPI	71.20%	Not-GPI	0.994
Dpr7	Not-GPI	34.80%	Not-GPI	0.508
Dpr8	Not-GPI	64.00%	Not-GPI	0.885
Dpr9	Not-GPI	71.20%	Not-GPI	0.995
Dpr10	Not-GPI	50.70%	Not-GPI	0.989
Dpr11	GPI	99.60%	GPI	0.341
Dpr12	GPI	99.90%	GPI	0.542
Dpr13	Not-GPI	45.20%	Not-GPI	0.922
Dpr14	Not-GPI	21.10%	Not-GPI	0.831
Dpr15	Not-GPI	67.70%	Not-GPI	0.992
Dpr16	Not-GPI	47.80%	Not-GPI	0.305
Dpr17	Not-GPI	57.20%	Not-GPI	0.793
Dpr18	Not-GPI	10.10%	Not-GPI	0.612
Dpr19	Not-GPI	98.90%	Not-GPI	0.352
Dpr20	Not-GPI	90.90%	Not-GPI	0.338
Dpr21	GPI	99.90%	GPI	0.283
DIP-α	Not-GPI	98.60%	GPI	0.301
DIP-β	Not-GPI	14.50%	Not-GPI	0.941
DIP-γ	GPI	100.00%	GPI	0.686
DIP-δ	GPI	100.00%	GPI	0.432
DIP-ε	GPI	99.60%	GPI	0.45
DIP-ζ	GPI	99.90%	GPI	0.643
DIP-η	Not-GPI	1.00%	GPI	0.422
DIP-θ	Not-GPI	74.80%	Not-GPI	0.606
DIP-ι	Not-GPI	98.80%	Not-GPI	0.501
DIP-κ	Not-GPI	25.90%	Not-GPI	0.992
DIP-λ	Not-GPI	9.10%	Not-GPI	0.802
Klingon	Not-GPI	98.50%	GPI	0.486

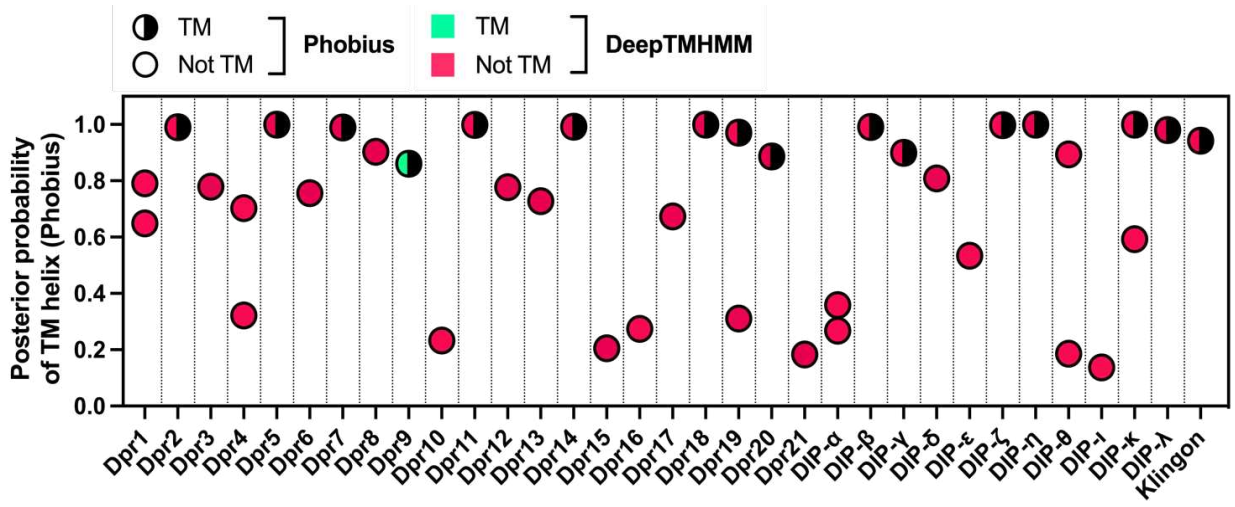

Figure S1. Transmembrane region prediction by Phobius and DeepTMHMM. Plotted are the highest values of posterior probability of a TM helix reported from Phobius. In cases where there were two regions with posterior probability of TM helix above 0.1, the highest values for both were plotted. TM, transmembrane. The highest values of posterior probability in Phobius do not always correlate with positive prediction for a given protein (Käll et al., 2007; for example, posterior probabilities of TM helix for Dpr8 or DIP-θ are higher than the one for Dpr9, but the former two were not predicted by Phobius to have a TM helix).

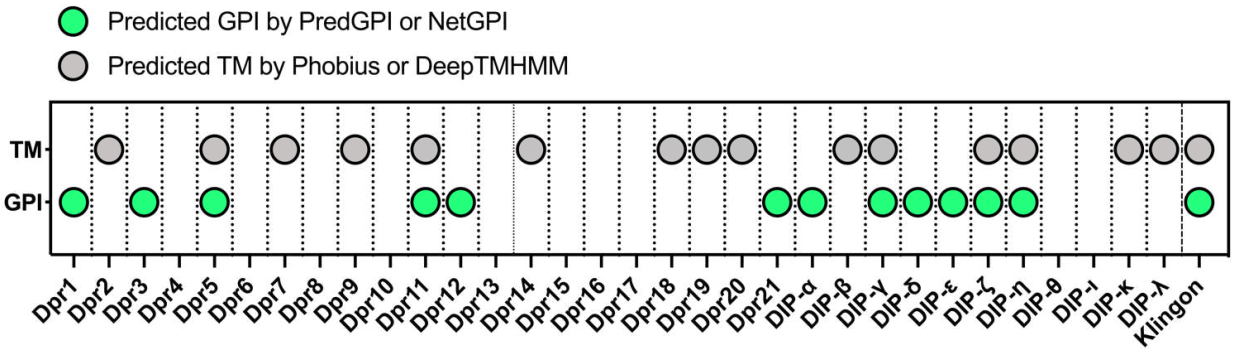

Figure S2. Summary of GPI anchor and TM helix predictions.

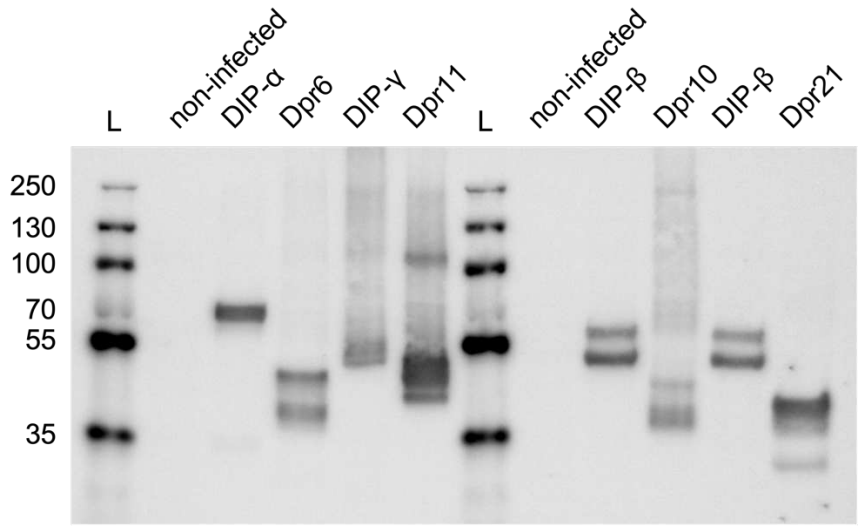

Figure S3. Expression of V5-tagged Dprs and DIPs in Sf9 cells used in cell aggregation assays. Sf9 cell pellets were solubilized and used in western blot with anti-V5-Alexa Fluor 647 antibody. L, molecular weight ladder.

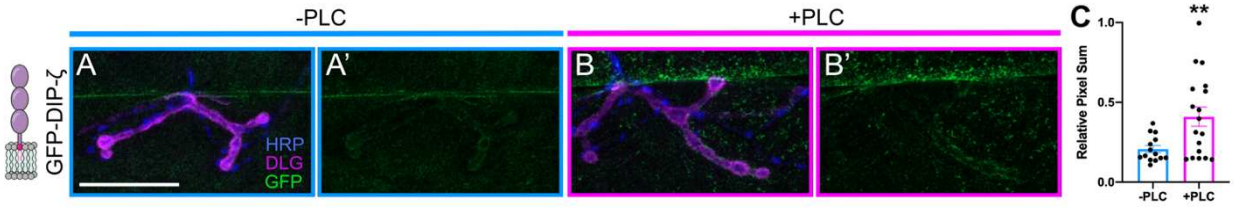

Figure S4: DIP-ζ aggregates in response to PLC treatment. (A-B') Tagged DIP-ζ was expressed in muscles and dissected larvae were treated with PLC and compared to non-treated controls. Cartoon of tagged DIP-ζ is shown in left column. Surface localized DIP-ζ is shown in green, neuronal tissue in blue (HRP), and postsynaptic membrane in magenta (DLG). (A-B) PLC efficiently increased surface labeling of V5 on muscles expressing EGFP-DIP-ζ. Scale bar = 50 μm. (C) Quantification of experiments shown in A-B'.